

Ab initio study of the modification of elastic properties of α iron by hydrostatic strain and by hydrogen interstitials

D. Psiachos,¹ T. Hammerschmidt,¹ and R. Drautz¹

¹*ICAMS, Ruhr-Universität Bochum, Bochum, Germany*

The effect of hydrostatic strain and of interstitial hydrogen on the elastic properties of α -iron is investigated using *ab initio* density-functional theory calculations. We find that the cubic elastic constants and the polycrystalline elastic moduli to a good approximation decrease linearly with increasing hydrogen concentration. This net strength reduction can be partitioned into a strengthening electronic effect which is overcome by a softening volumetric effect. The calculated hydrogen-dependent elastic constants are used to determine the polycrystalline elastic moduli and anisotropic elastic shear moduli. For the key slip planes in α -iron, $[1\bar{1}0]$ and $[11\bar{2}]$, we find a shear modulus reduction of approximately 1.6% per at.% H.

I. INTRODUCTION

Hydrogen degrades the performance of many alloys and steels by lowering the failure stress, leading to fracture at unpredictable loading conditions^{1,2}. Several mechanisms have been proposed to explain the H-embrittlement of iron, the main ones being the hydrogen-enhanced decohesion (HEDE) mechanism^{3,4}, H-vacancy effects⁵⁻⁷, and hydrogen-enhanced localised plasticity (HELP)⁸⁻¹⁰.

In the HEDE mechanism, H weakens the cohesive bonds between the metal atoms, leading to failure at interfaces where H tends to concentrate in, such as around the tensile strain field of a crack opening^{3,4}. Vacancies containing H can order themselves along critical slip directions, leading to fracture^{6,7}. Within the HELP mechanism, the onset of plasticity with loading occurs at a lower stress as a result of the H-shielding of repulsive interactions between dislocations⁹. The increased H concentration at dislocations¹¹ effectively reduces the dislocation-dislocation spacings. The resulting phenomenon of dislocation coalescence, and ultimately, crack advancement at reduced loads, in the presence of H, may be related to the experimentally-observed increase of dislocation mobility caused by H¹⁰. The importance of increased H-concentration near dislocations and other low-energy trap sites such as interstitial sites was also indicated by a recent experimental study of intergranular failure in steel¹². In that study, the fracture mode changed from ductile to brittle, as the amount of H located at these low-energy trap sites increased.

One of the central challenges in avoiding hydrogen embrittlement is the interpretation of the experimentally observed effective behaviour¹²⁻¹⁵ that arises from the interplay of H solubility and diffusivity with cohesive/elastic properties, vacancies, dislocations, and other defects. The advantage of theoretical approaches is that the effects can be investigated independently, in contrast to experiment. Combining highly-accurate electronic structure calculations¹⁶⁻¹⁸ with other methods enables access to extended time and length scales which are necessary for describing e.g. long-range strain fields or small H concentrations¹⁹, kinetic effects^{20,21} and for

predicting continuum-scale properties^{22,23}.

The goal of this study is to establish a link between highly-accurate *ab-initio* calculations and continuum elasticity-theory in order to explain the experimentally-observed influence of hydrogen on the elastic properties of iron (*e.g.* Ref. 24) and steel (*e.g.* Ref. 25). To this end we use density-functional theory to calculate the elastic constants of α -Fe as a function of hydrostatic stress and different concentrations of interstitial hydrogen.

In Sec. II we describe the details of our DFT calculations used to calculate the elastic constants of pure Fe (Sec. III) and the modification of the elastic constants by H (Sec. IV). We utilize the elastic constants to calculate the effect of H on the strength parameters - bulk, Young's, and shear moduli - in Sec. V and summarise our findings in Sec. VI.

II. DETAILS OF THE CALCULATIONS

A. *Ab initio* total energies

The calculation of elastic properties presented here is based on numerical derivatives of the total energy with respect to strain. The large unit cells required for reaching H concentrations of a few percent makes this problem just within the scope of present DFT calculations.

Our spin-polarised first-principles density functional theory calculations were performed using the VASP²⁶⁻²⁸ code. We used the projector augmented-wave method^{29,30}, with pseudopotentials considering the 3p electrons of Fe as valence electrons. The generalised gradient approximation (GGA) in the PW91 parametrisation³¹ was used for the exchange-correlation functional. In order to verify the reliability of our conclusions, we repeated some of our calculations with the Vosko-Wilk-Nusair³² (VWN) spin interpolation in PW91, and the Perdew-Burke-Ernzerhof³³ (PBE) exchange-correlation functional. The spin-polarised GGA has proven to give reliable results for the ground state³⁴ and elastic properties³⁵ for Fe.

We used supercell geometries, a plane-wave basis with a cutoff of 500 eV and a Γ -centred k-point grid equivalent

to $18 \times 18 \times 18$ for the two-atom basis bcc unit cell except in the case of the 128-atom unit cell where the Brillouin-zone sampling was equivalent to $20 \times 20 \times 20$. We found these settings to be more than adequate for capturing the equilibrium properties, but necessary for converging the elastic constants to within less than one percent error (see Sec. III B). The ions were relaxed until the maximum force component on each ion was less than $0.01 \text{ eV}/\text{\AA}$ while the total energies were converged to within 0.01 meV . The reported lattice parameter was determined from fitting the total energies to the Murnaghan equation of state³⁶.

Our results for the lattice parameter (2.832 \AA), bulk modulus (194 GPa), bulk-modulus pressure derivative (5.42), and magnetic moment ($2.17 \mu_B$) are in good agreement with other first-principles calculations^{37–40} and with experimental results^{41,42}.

III. ELASTIC CONSTANTS

A. General description and convergence criteria

The total energy of a solid at zero stress and equilibrium volume V_0 can be expanded about small strains ϵ

$$E(\epsilon) = E(0) + \frac{1}{2!} V_0 \sum_{ijkl} C_{ijkl} \epsilon_{ij} \epsilon_{kl} + \dots \quad (1)$$

where the indices run from 1-3. As the strain tensors are symmetric, the notation C_{ijkl} can be expressed in the two-index (Voigt) form C_{ij} where the indices run from 1-6. In this section we restrict ourselves to linear elastic behaviour, *i.e.* stress linear in the strain.

For the calculation of the elastic constants in this work, we enforced cubic symmetry of the unit cells in our DFT calculations. This reflects our expectation that a random distribution of H would cause an effectively isotropic lattice distortion. In addition, the restriction to cubic volume elements facilitates the scale-bridging with mesoscopic approaches, such as *e.g.* finite element schemes. In Sec. IV B we will show that the quantitative effect of this cubic constraint is in fact negligible for the investigated unit cells.

Within our approximation of a cubic system, the number of independent elastic constants C_{ij} reduces to three: C_{11} , C_{12} , and C_{44} . Their numerical values can be determined by applying suitable strain tensors and taking the second derivative of Eq. 1 with respect to the applied strain. The bulk modulus $B = \frac{1}{3}(C_{11} + 2C_{12})$ and its pressure derivative $B'(P)$ are found by applying hydrostatic strains and then carrying out a fit to the Murnaghan equation of state. The values of $C' = C_{11} - C_{12}$ and C_{44} are found by applying volume-conserving strains.

In the case of C' , an orthorhombic strain

$$\epsilon = \begin{pmatrix} \delta & 0 & 0 \\ 0 & -\delta & 0 \\ 0 & 0 & \delta^2/(1-\delta^2) \end{pmatrix} \quad (2)$$

is applied, giving a total energy expression

$$E_{ortho.}(\delta) = E(0) + C'V\delta^2 + O[\delta^4], \quad (3)$$

while, for C_{44} , the strain is monoclinic

$$\epsilon = \begin{pmatrix} 0 & \delta/2 & 0 \\ \delta/2 & 0 & 0 \\ 0 & 0 & \delta^2/(4-\delta^2) \end{pmatrix}. \quad (4)$$

with a total energy

$$E_{mono.}(\delta) = E(0) + \frac{1}{2}C_{44}V\delta^2 + O[\delta^4]. \quad (5)$$

We fitted our *ab initio* total energies for systems subject to nine values of strain δ between $\pm 3\%$ to Eqs. 3 and 5 in order to obtain C' and C_{44} .

B. Convergence tests

To estimate the accuracy of the elastic-constant calculations, we carried out extensive convergence tests. The quantities varied were the k-point density, cutoff energy, and strain δ at a lattice parameter of 2.832 \AA . An example of these convergence tests is shown in Fig. 1a for C_{44} , for $|\delta| \leq 3\%$ (the convergence tests for C' are similar). The values of cutoff energy and k-point density of the circled point (500 eV , $18 \times 18 \times 18$) were used in (b) and (c) to verify that the applied strains are within the linear regime.

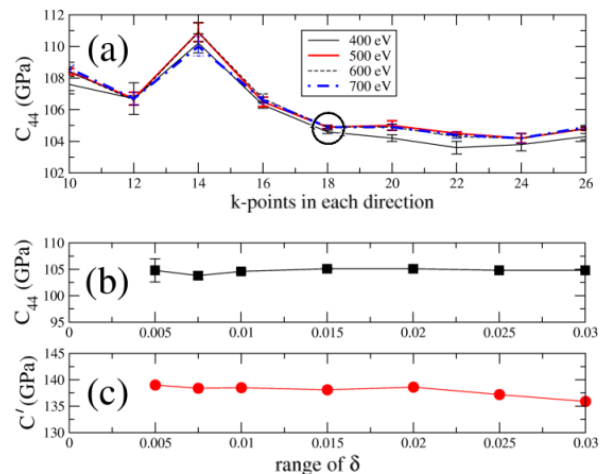


FIG. 1: (a) Convergence of C_{44} as a function of k-point density and energy cutoff for the two-atom bcc-Fe cell for a range of strain values $|\delta| \leq 3\%$ (see Eqs. 2-5). The error bars are deduced from the least-squares fit to Eq. 5. The circled point corresponds to the calculation parameters used in this study. (b) C_{44} and (c) C' obtained for different ranges of strain δ .

As a result of our extensive convergence tests, we observed less than a 2% variation in the elastic constants upon varying the range of δ between 0.5-3% change in δ .

For the calculations presented in the remainder of this study, we chose a value of 3% for δ , *i.e.* at the border of linear elastic behaviour, in order to avoid numerical instabilities and/or the need for very high precision total energy evaluations.

C. Dependence of elastic constants on hydrostatic strain

In order to achieve a comprehensive description of the influence of volume-expansion due to interstitial H, we also investigated the nonlinear elastic behaviour of the elastic constants of pure Fe as a function of hydrostatic strain. Equivalently, this is the effect of a volume expansion on the linear elastic constants C_{ij} . The modified second-order elastic constants are given by Birch⁴³ in terms of the second-order and third-order elastic constants C_{ij} and C_{ijk} to linear order in the applied hydrostatic strain. Instead of calculating the third-order elastic constants, we directly determined the variation in the second-order elastic constants as a function of small applied hydrostatic strain.

Following Wallace [44], the total energy at a volume V produced by strains applied at a reference volume V^{ref} away from equilibrium, is modified from Eq. 1 to include a term first-order in strain, corresponding to hydrostatic stress σ_{ij} :

$$E(V, \epsilon) = E(V^{ref}, \epsilon = 0) + V^{ref} \sum_{ij} \sigma_{ij} \epsilon_{ij} + \frac{V^{ref}}{2} \sum_{ijkl} \epsilon_{ij} C_{ijkl}(V^{ref}) \epsilon_{kl}. \quad (6)$$

Formally, the strains are Lagrangian (second-order in displacement) strains evaluated with respect to V^{ref} (as in Eq. 2.37 in [44]) but, as we are only concerned with small strains, we approximate them as infinitesimal.

Because the stress is hydrostatic, it can be written as $\sigma_{ij} = -P\delta_{ij}$. Expanding Eq. 6 and allowing the strains represented by Eqs. 2 and 4 to be applied with respect to V^{ref} , we obtain

$$E_{ortho.}(P, \delta) = E(P, 0) + (C' - P) V^{ref} \delta^2 + O[\delta^4], \quad (7)$$

$$E_{mono.}(P, \delta) = E(P, 0) + \frac{1}{2} \left(C_{44} - \frac{P}{2} \right) V^{ref} \delta^2 + O[\delta^4]. \quad (8)$$

as modifications of Eqs. 3 and 5, where we have removed the V^{ref} functional dependence notation from the C_{ij} for clarity.

However, the elastic constants of Eq. 6, henceforth known as the energy-strain coefficients, even while modified to be valid at V^{ref} , are no longer equal to the stress-strain coefficients. This is discussed in detail by Wallace⁴⁴ (Eq. 2.51) and Barron and Klein⁴⁵. Experiments mostly use either ultrasonic wave-propagation⁴⁶

or diffraction techniques^{47,48} and obtain the pressure-varying elastic constants from stress-strain relations. The stress-strain coefficients, which we call $\overset{\circ}{c}_{ijkl}$ as in Ref. 45, are related to the energy-strain coefficients C_{ijkl} of Eq. 6 by

$$\overset{\circ}{c}_{ijkl} = C_{ijkl}(V^{ref}) + \frac{1}{2} P (2\delta_{ij}\delta_{kl} - \delta_{il}\delta_{jk} - \delta_{ik}\delta_{jl}), \quad (9)$$

or in simplified terms

$$\begin{aligned} \overset{\circ}{c}_{11} &= C_{11} \\ \overset{\circ}{c}_{12} &= C_{12} + P \\ \overset{\circ}{c}_{44} &= C_{44} - \frac{1}{2} P. \end{aligned} \quad (10)$$

We note here that the expressions 9-10 differ from those found in works which consider Lagrangian strains^{49,50} but agree with others also using infinitesimal strains⁵¹⁻⁵³. One consequence of using the stress-strain coefficients instead of the energy-strain coefficients is that Eqs. 3 and 5 retain their form, apart from the replacement of the C' and C_{44} by $\overset{\circ}{c}' \equiv \overset{\circ}{c}_{11} - \overset{\circ}{c}_{12}$ and $\overset{\circ}{c}_{44}$ respectively. We use the stress-strain coefficients $\overset{\circ}{c}_{ijkl}$ in order to avoid ambiguities in the definition of the C_{ijkl} at non-zero pressure when comparing with experiments, or with other computational studies.

At each value of hydrostatic strain η ranging between ± 0.05 , the value of δ was varied between ± 0.03 and a fit was made to second-order in δ , as in Sec. III A. These applied strain values correspond to the initial linear regime of the high-pressure transition to the body-centred-tetragonal phase⁵¹. The elastic constants $\overset{\circ}{c}'$ and $\overset{\circ}{c}_{44}$ are again extracted from the coefficients of δ^2 . However, in order to separate $\overset{\circ}{c}_{11}$ and $\overset{\circ}{c}_{12}$ from $\overset{\circ}{c}'$, we need to take into account the change of the bulk modulus with pressure. The bulk modulus is modified by a term equal to its pressure derivative $B'(P)$ multiplied by the pressure at the corresponding value of hydrostatic strain η . The resulting variation of the stress-strain coefficients with hydrostatic strain follows a linear trend, as can be seen from Fig. 2. A linear least-squares fit to the small-

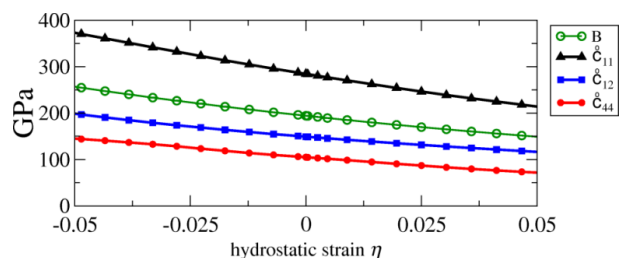


FIG. 2: Calculated stress-strain coefficients for pure Fe as a function of hydrostatic strain $\eta = \Delta V/V_0$ with respect to the equilibrium volume V_0 .

strain region ($|\eta| < 0.02$) of these curves resulted in the

following dependence of the stress-strain coefficients on hydrostatic strain:

$$\begin{aligned}
 B(\eta) &= (194 - 1075\eta) \text{ GPa} \\
 \overset{\circ}{c}_{11}(\eta) &= (284 - 1492\eta) \text{ GPa} \\
 \overset{\circ}{c}_{12}(\eta) &= (149 - 887\eta) \text{ GPa} \\
 \overset{\circ}{c}_{44}(\eta) &= (105 - 662\eta) \text{ GPa}
 \end{aligned} \tag{11}$$

and the corresponding hydrostatic strain dependence of the energy-strain coefficients was

$$\begin{aligned}
 C_{11}(\eta) &= (284 - 1492\eta) \text{ GPa} \\
 C_{12}(\eta) &= (149 - 669\eta) \text{ GPa} \\
 C_{44}(\eta) &= (105 - 761\eta) \text{ GPa}.
 \end{aligned} \tag{12}$$

The difference between the stress-strain and energy-strain coefficients is quite small, and virtually indiscernible on the scale of Fig. 2. Additionally, the use of another exchange-correlation functional (PW91+VWN, PBE) changed the absolute values of the energy-strain coefficients, but it had a negligible effect on the slopes of Fig. 2.

Previously-reported first-principles calculations of the stress-strain dependence of bcc-Fe (Tab. I) show a spread of approximately 10% and tend to overestimate the experimental values for $\overset{\circ}{c}_{11}$ and $\overset{\circ}{c}_{12}$ while underestimating $\overset{\circ}{c}_{44}$. This spread may be attributed to *e.g.* different exchange-correlation functionals, applied strains, or criteria for convergence. We did an interpolation of the previously published data to obtain the values listed for the strain-dependences in the table. Experimental data

method	$\overset{\circ}{c}_{11}$ (GPa)	$\overset{\circ}{c}_{12}$ (GPa)	$\overset{\circ}{c}_{44}$ (GPa)
PAW-GGA (present)	284(-1492)	149(-887)	105(-662)
PAW-GGA ⁵⁴	271(-1228)	145(-535)	101(-454)
LMTO-GGA ⁵⁵	303(-1282)	150(-813)	126(-604)
PP-GGA ⁵⁶	289	118	115
FP-LAPW ⁵¹	285	139	100
expt. ⁴¹	245	139	122
expt. ⁵⁷	240	136	121

TABLE I: Comparison of stress-strain parameters (and their hydrostatic strain η dependence in parentheses, if available) obtained in the present study (Eq. 11) with other calculations, and with experimental results.

points⁴⁶⁻⁴⁸ for the hydrostatic-strain dependencies of the stress-strain coefficients are displayed along with the calculated results by Sha and Cohen⁵⁵ in their paper, and these agree well with their calculations. Our derivatives do not deviate appreciably compared to the other results.

It is worth noting that the elastic moduli for a wide variety of phases of Fe have been found to decrease with applied compressive strain⁵⁸.

IV. DEPENDENCE OF ELASTIC CONSTANTS ON H-CONCENTRATION

A. Simulation cells

The elastic constants of pure Fe serve as a starting point for determining the influence of interstitial H atoms on the elastic properties. In this study, we focus on interstitial H in the tetrahedral site (Fig. 3) because (i)

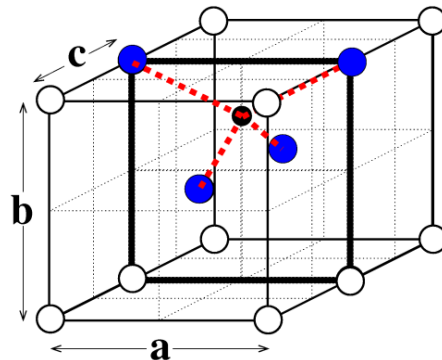


FIG. 3: Location of an H atom in the tetrahedral interstitial position on the face between two bcc unit cells. Lines towards nearest-Fe neighbours (blue circles) are shown.

we find this site to be 0.13 eV more stable than the octahedral one at zero stress (in agreement with previous DFT studies^{16,17}) and (ii) we expect that the twice as large number of tetrahedral sites (compared to octahedral sites) per Fe atom will dominate the mechanical properties at ambient temperatures. We implement the variation of H-concentration in the supercell approach of our calculations by (i) increasing the size of a supercell containing one H atom, or by (ii) adding a second H atom to the same supercell. In addition, we changed the symmetry of the supercell or the position of the second H atom relative to the first in order to alter the ordering of the H atoms within the Fe host lattice. The dimensions of supercells and number of H atoms used to achieve various H concentrations are listed in Tab. II. For each of these supercells we determined the elastic constants by assuming a cubic lattice but, by allowing for internal ionic relaxations, accounting in an approximate way for the local distortions due to H.

B. Effect of non-cubic distortions

The volume expansion of the Fe host lattice by H in the tetrahedral interstitial site introduces distortions which break the cubic symmetry. For the H-orientation shown in Fig. 3, the Fe nearest-neighbours expand radially-outward from H (along the red lines), resulting in a total expansion, when projected onto the cube axes, identical in the *a* and *c* directions, and greater than that along *b* (see *e.g.* Ref. 59). This tetragonal distortion

at. % H	n(H)	$k \times l \times m$
0	0	1×1×1
0.8	1	4×4×4
1.8	1	3×3×3
2.7	1	3×3×2
3.6	2	3×3×3
4.0	1	2×2×3
5.3	1	3×3×1
5.9	1	2×2×2
5.9	1	2×4×1
7.7	1	1×2×3
10.0	2	3×3×1
11.1	2	2×2×2

TABLE II: Investigated H-concentrations with corresponding number of H atoms, $n(\text{H})$, and supercell dimensions in multiples k , l , and m of the two-atom bcc Fe cell. For the highest concentration (11.1 at.%) we considered three configurations with H-H spacings within the supercell of 4.98 Å, 3.66 Å, and 2.31 Å.

increases the number of unique elastic constants from three to six: $C_{12} = C_{23} \neq C_{13}$, $C_{11} = C_{33} \neq C_{22}$, and $C_{44} = C_{66} \neq C_{55}$. The variation among the no-longer equivalent elastic constants depends on the degree of tetragonal distortion, which is affected by increasing H-concentration and additionally may be broken depending on the relative H positions in the supercell.

In order to justify our use of a cubic cell, we compared our results with those from a tetragonal unit cell for one of the most distorted cases considered in our study, a tetragonal distortion $b/a - 1$ of -0.4%, obtained at an H concentration of 11.1 atomic % and H-H spacing within the supercell of 4.98 Å. Despite the presence of two H in the simulation cell, the distortion was tetragonal. The lattice parameters of the tetragonal unit cell were obtained from a quadratic fit over a two-dimensional grid of total energies.

The elastic constants for the explicitly tetragonally-distorted unit cell at 11.1 at. % were calculated using the strain and total energy expressions given in Ref. 60. For the cubic unit-cell, the elastic constants were explicitly calculated by straining in the different Cartesian directions and averaging. Table III summarises the average values of the cubic and tetragonal elastic constants along with the associated standard errors computed from the spread in the values for the different orientations. Only

	cubic	tetragonal
$\bar{C}_{11} = \frac{1}{3}(C_{11} + C_{22} + C_{33})$	240±7	239±6
$\bar{C}_{12} = \frac{1}{3}(C_{12} + C_{13} + C_{23})$	145±3	147±15
$\bar{C}_{44} = \frac{1}{3}(C_{44} + C_{55} + C_{66})$	92±2	93±2

TABLE III: Elastic parameters (GPa) for the highest-considered H-concentration (11.1 at.%) as obtained for a cubic or tetragonal ($b/a-1=-0.4\%$) unit cell.

\bar{C}_{12} gave a large spread for the tetragonal cell (separately, the values were $C_{12} = C_{23}=138$ GPa, $C_{13}=164$ GPa) but not for the cubic cell. The excellent agreement be-

tween the elastic constants of the tetragonal and cubic cells is not surprising, as the cell volumes were found to be the same, which caused the variations in the elastic constants arising from different lattice parameters (details in Sec. III C) in the tetragonal cell to mostly average out in the cubic cell. As a result of the excellent agreement with the cubic approximation for this highly-distorted case, we are confident that our results for all concentrations obtained with the cubic cell accurate. For the cubic unit cells with an H-concentration of greater or equal to 4 at.%, the elastic constants were explicitly calculated by straining in the different Cartesian directions and then averaged. For lower concentrations, as the spread amongst the three directions was $< 2\%$, there was no averaging done. Instead, the associated errors are from the least-squares fitting of the total energy as a function of strain.

C. Single-crystal elastic constants

The calculated variation of cubic elastic constants with H concentration is shown in Fig. 4. Additional data points at the same concentration correspond to differently-ordered structures (see Tab. II). There is a

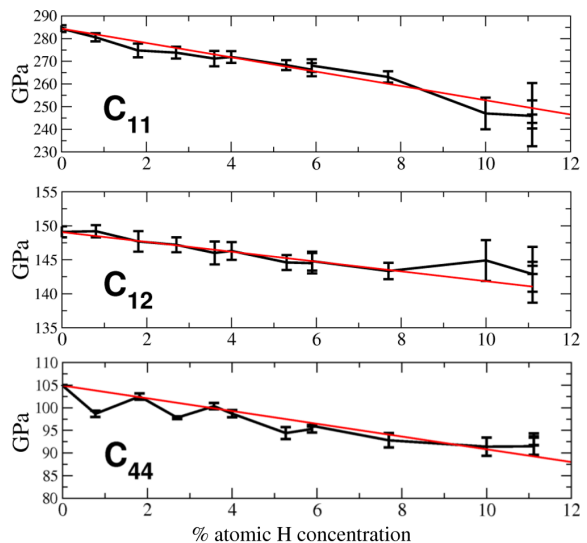


FIG. 4: Calculated elastic constants for bcc Fe as a function of H concentration, along with a line of best fit to the $\leq 7.7\%$ points (see text for an explanation regarding the outlying points).

clear trend of decreasing elastic constants with increasing H concentration. We ascribe the outlying values of C_{11} and C_{12} for the 10 % concentration to the high stress associated with the particular relative orientation of the two H atoms, and also because of their proximity to their periodic images in the smallest dimension. The spread at 11.1% is hidden in the error bars associated with the non-cubic distortions. At the other concentration, 5.9%, for which we examined different orderings, there was no sig-

nificant difference between the values. We constrained the lines of best fit shown in Fig. 4 to pass through the zero-concentration value, but we neglected the data points above 7.7% and the 0.8% value of C_{44} . These lines of best fit, as a function of atomic H concentration x , are given by

$$\begin{aligned} C_{11}(x) &= (284 - 316x) \text{ GPa} \\ C_{12}(x) &= (149 - 72x) \text{ GPa} \\ C_{44}(x) &= (105 - 141x) \text{ GPa}. \end{aligned} \quad (13)$$

Calculations with an embedded-atom potential of the modification of elastic moduli of Fe by H have been reported recently in Ref. 61. The data covered up to 6 at.% H and while the elastic moduli decreased with H initially, the effect levelled off with increasing H and generally was far weaker than here.

Given the pressure-dependence of the elastic constants (*e.g.* Ref. 51), one would expect that part of the observed modification of elastic properties with H concentration can be attributed to the volumetric effect of the interstitial H on the Fe host lattice. In our calculations, the volumetric effect of H is immediately apparent through the linear increase of supercell volume with H concentration shown in Fig. 5. From the slope, we determined that each H expands the lattice by 4.5 \AA^3 , in excellent agreement with the value 4.4 \AA^3 obtained from experiment⁶². This relation enables us to express the H concentration in

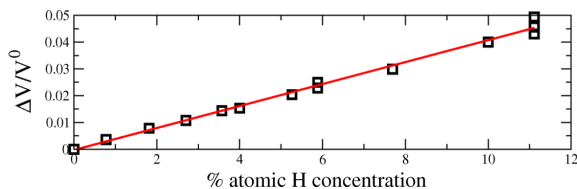


FIG. 5: Relative volume expansion as a function of H concentration where ΔV is the volume difference of the system with H compared with the volume V^0 of pure Fe.

terms of a volume change corresponding to a hydrostatic strain η which we can employ in our parametrisation of the elastic constants (Eq. 11). This corresponds to a direct evaluation of the volumetric effect of H on the elastic constants. The volume-induced changes in elastic properties are shown in Fig. 6, together with the total effects originally displayed in Fig. 4. By taking the difference of H-dependence and volume-dependence, we remove the contribution of strain of pure Fe from the elastic parameters calculated at the equilibrium volume corresponding to each concentration of H. The resulting difference plots (dashed lines in Fig. 6) show the residual effects, which include electronic contributions, of H at each concentration (and implicit corresponding volume).

The separation of solute effects from alloy elastic moduli has been also considered in Ref. 63 for H in Nb, and by Ref. 64 for different Fe-based binary alloys. In these studies, the volume effect was parametrised, by the equiv-

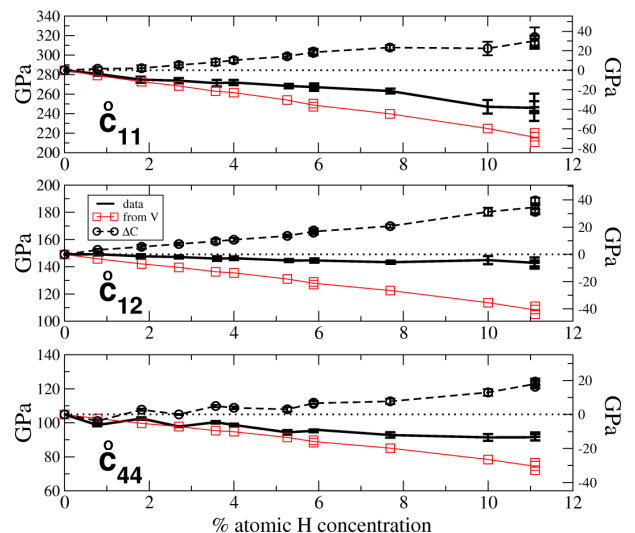


FIG. 6: Left vertical axis scale: Variation of stress-strain coefficients with H (data from DFT - same as in Fig. 4) and volume-expected variation (parametrised from pure iron - see Eq. 11). Right vertical axis scale: difference between total and volume effect (dashed lines).

alent of a line of best fit to the data of Fig. 5, whereas we determined it explicitly using the individual data points.

V. DEPENDENCE OF STRENGTH PARAMETERS ON H CONCENTRATION

A. Polycrystalline elastic moduli

Single-crystal Fe samples with H are difficult to prepare while the measurements of the C_{ij} do not directly relate to the strength properties of the material. Most samples are polycrystalline, and typical measurements are directly related to stiffness (bulk modulus), tensile strength (Young's modulus), and hardness (shear modulus). In addition, microscopic simulations such as finite-element calculations, whose inputs consist of polycrystalline averages of elastic moduli, can make direct comparisons with such experiments. Therefore, we transformed our single-crystal results to polycrystalline Fe by using combinations of the stress-strain coefficients C_{ij} to derive various elastic moduli for describing different types of stress-strain responses. Shown in Fig. 7 are the bulk modulus, and the polycrystalline averages of the Young's and shear moduli, where the average was performed according to the expression by Hill, which is an average of the Voigt and Reuss bounds⁶⁵. As in Fig. 6, the volumetric changes in the moduli for pure Fe are also shown. We find a clear trend in the elastic regime towards a stiffening (B increased), tensile strengthening (E increased), and hardening (G increased) of the system with increasing concentration of H. Despite the overall softening of the material with increasing H concentration, our find-

ings indicate that H weakens the softening caused by the accompanying volume expansion. Our overall findings

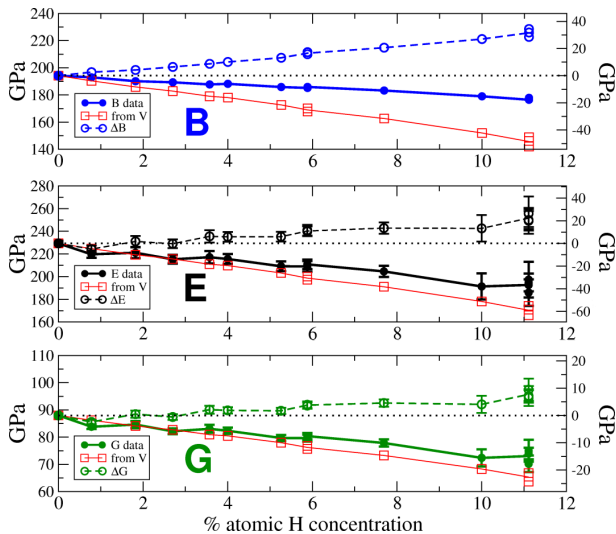


FIG. 7: Left vertical axis scale: Variation of polycrystalline moduli (B- bulk, E-Young’s, G-shear) with H (data from DFT) and volume-expected variation (parameterised from pure iron - see Eq. 11). Right vertical axis scale: the difference between total and volume effect (dashed lines).

are in reasonable agreement with the experimentally deduced decrease of the shear modulus of polycrystalline Fe by 8% for 1 at% H⁶⁶.

The effect of H on the mechanical properties of iron has been controversial. A study by Matsui *et al*⁶⁷ found that in tensile tests, the flow stress is increased at low temperatures by H whereas at higher temperatures it found softening. The study indicated that the H-dislocation interaction plays an important role in determining the type of effect that H has on the mechanical properties. Specifically, whether the presence of H results in the hindering or enhancing (as in HELP) of dislocation mobility, seems to determine whether the effect is material hardening or softening respectively⁶⁷. A very recent discussion of this controversy, which continues to persist, is given in Ref. 68. It is important to note that the above-mentioned studies dealt with austenitic (fcc) steel, and that similar experiments on ferritic (bcc) steel cannot easily be conducted due to the much greater diffusivity of H in bcc versus fcc iron⁶⁸.

B. Shear moduli in key slip planes

Our H and volume-dependent elastic constants also enable us to more closely study macroscopic failure mechanisms. Therefore, we determine the H dependence of the shear modulus, an important quantity for describing the stress needed for dislocation nucleation¹⁴ and glide⁶⁹. The shear modulus describes the elastic stress response to applied shear strain. In a single-crystal sample, the elas-

tic moduli are anisotropic, meaning they take on different values when rotated to a different coordinate frame than the standard [100] orientation used in earlier sections.

The shear modulus is defined by

$$G_{ij} \equiv \frac{\sigma_{ij}}{\epsilon_{ij}}; \quad i \neq j; \quad i, j = 1, 2, 3 \quad (14)$$

where the indices 1,2,3 denote the x, y, z axes of the coordinate system. The transformation of strains from the reference (unprimed) to rotated (primed) coordinate system can be performed using Euler angles or direction cosines (see *e.g.* Ref. 70). The rotated strains hence become $\epsilon' = \mathbf{T}\epsilon\mathbf{T}^T$ where \mathbf{T} is the transformation matrix for transforming the reference coordinates \mathbf{x} into the new frame $\mathbf{x}' = \mathbf{T}\mathbf{x}$. Simplified expressions for the directionally-dependent shear modulus are given in Ref. 71, whose notation we follow.

Using the lines of best fit for the concentration-dependent elastic constants of (Fig. 4), we are able to parametrise the different shear moduli as a function of concentration for arbitrary planes and strain directions. The atomic displacements during a shear distortion constitute slip, and in bcc metals, the most common direction of slip is the closest-packed $\langle 111 \rangle$ direction with the main slip planes being $\{110\}$ and $\{112\}$ ⁶⁹.

The two major shear moduli for cubic symmetry are G_{23} and G_{12} . The G_{23} shear modulus describes $y'z'$ shear. The diagram in the upper part of Fig. 8 shows the coordinate system for an arbitrary plane defining the x' , or $\mathbf{1}$ axis. It contains a degree of freedom, θ , defining the orientation of the $\mathbf{2}$ and $\mathbf{3}$ axes in the plane normal to the $\mathbf{1}$ axis. G_{12} is the shear modulus when $x'y'$ shear is applied.

We display the directionality of the shear moduli as polar plots in Fig. 8 for the two key slip planes of bcc-Fe. The shear modulus G_{23} for pure Fe in the $[1\bar{1}0]$ plane has a maximum for slip in the $\langle 001 \rangle$ and $\langle 110 \rangle$ direction. The minimum, at $\theta = 45^\circ$, does not correspond to any integer-multiple direction; the nearest one being $\langle 111 \rangle$ at $\theta \approx 35^\circ$, which is the expected direction of slip. For the $[11\bar{2}]$ plane, the minimum is also the $\langle 111 \rangle$ direction. The values of G_{23} and G_{12} are the same for some directions but different in others. They are competing with each other when deciding which plane is most susceptible to slip and in which direction. For example, looking only at G_{23} of the $[11\bar{2}]$ plane (Fig. 8b), it appears that both the $\langle 111 \rangle$ and $\langle 1\bar{1}0 \rangle$ are equally soft, but $\langle 111 \rangle$ prevails in softness when G_{12} is examined. With increasing H-concentration, we find a nearly uniform, linear decrease in the shear modulus in all θ directions. The dependence on θ is weak and not visible on the scale of Fig. 8. We find a similar rate of decrease for all planes, amounting to an average over θ of $1.6 \pm 0.1\%$ per atomic % H.

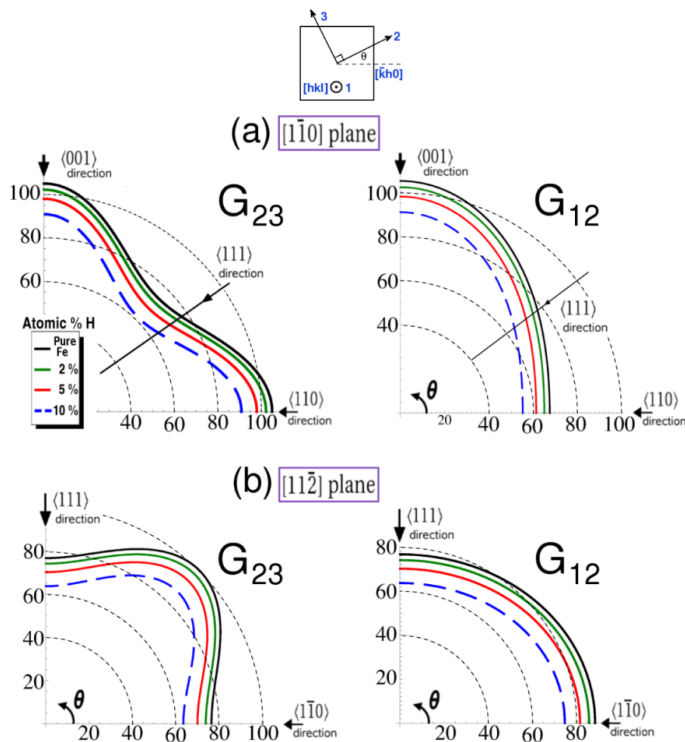


FIG. 8: Directional dependence of the shear moduli G_{23} and G_{12} (in GPa) for the slip planes (a) $[1\bar{1}0]$ and (b) $[11\bar{2}]$ of bcc-Fe, for different values of H concentration. The angle θ is the degree of freedom in the choice of axes in the shear plane (inset).

VI. CONCLUSIONS

We have studied the modification of the elastic properties of bcc Fe by hydrostatic strain and by interstitial hydrogen. The calculations were carried out for hydrogen concentrations between 0.8 at.% and 11.1 at.% with simulation cells of different dimensions. Our applied constraint of a cubic lattice was verified by a comparison

with a tetragonally-distorted unit cell at the highest investigated hydrogen concentration.

From our density-functional theory calculations, we observe a significant linear decrease of the elastic constants C_{11} , C_{12} and C_{44} with increasing hydrostatic strain or with increasing concentration of interstitial hydrogen. The volumetric part of the hydrogen dependence can be isolated by relating the volume dependence of the elastic constants to the volume expansion of the corresponding hydrogen concentration. The overall decrease in elastic constants is the result of two opposing contributions: the decrease in elastic constants with increasing volume per atom versus an increase from the electronic contribution. These opposing effects may help to reconcile contradictory experimental findings - hardening or softening - under different conditions and concentrations.

We used the elastic constants from our single-crystal *ab-initio* calculations to examine the dependence of the polycrystalline elastic moduli B , E , and G on the hydrogen concentration and find good agreement with the few available measurements. The single-crystal shear moduli G_{12} and G_{23} deduced from the *ab-initio* calculations show an isotropic decrease of approximately 1.6% per at.% H. This suggests that a lower yield stress (assuming the same yield strain) could be expected as a result of the H-lowered strength parameters in the investigated elastic regime.

Acknowledgements

We acknowledge financial support through ThyssenKrupp AG, Bayer MaterialScience AG, Salzgitter Mannesmann Forschung GmbH, Robert Bosch GmbH, Benteler Stahl/Rohr GmbH, Bayer Technology Services GmbH and the state of North-Rhine Westphalia as well as the European Commission in the framework of the ERDF.

- ¹ R. A. Oriani, *Corrosion* **43**, 390 (1987).
- ² J. P. Hirth, *Metall. Trans. A* **11**, 861 (1980).
- ³ A. R. Troiano, *Am. Soc. Met.* **52**, 54 (1960).
- ⁴ R. A. Oriani and P. H. Josephic, *Acta Metall.* **25**, 979 (1977).
- ⁵ M. S. Daw and M. I. Baskes, *Phys. Rev. Lett.* **50**, 1285 (1983).
- ⁶ Y. Tateyama and T. Ohno, *ISIJ Int.* **43**, 573 (2003).
- ⁷ Y. Tateyama and T. Ohno, *Phys. Rev. B* **67**, 174105 (2003).
- ⁸ C. D. Beachem, *Metall. Trans. A* **3**, 437 (1972).
- ⁹ H. K. Birnbaum and P. Sofronis, *Mat. Sci. Eng.* **A176**, 191 (1994).
- ¹⁰ I. M. Robertson, *Eng. Frac. Mech.* **68**, 671 (2001).
- ¹¹ A. H. Cottrell and B. A. Bilby, *Proc. Phys. Soc.* **62**, 49 (1949).
- ¹² P. Novak, R. Yuan, B. P. Somerday, P. Sofronis, and R. O. Ritchie, *J. Mech. Phys. Solids* **58**, 206 (2010).
- ¹³ W. W. Gerberich, D. D. Stauffer, and P. Sofronis, in *Effects of Hydrogen on Materials*, edited by B. Somerday, P. Sofronis, and R. Jones (ASM International, Materials Park OH, 2009), p. 38.
- ¹⁴ A. Barnoush and H. Vehoff, *Acta Mat.* **58**, 5274 (2010).
- ¹⁵ R. Kirchheim, *Scr. Mat.* **62**, 67 (2010).
- ¹⁶ D. E. Jiang and E. A. Carter, *Phys. Rev. B* **70**, 064102 (2004).
- ¹⁷ J. Sanchez, J. Fullea, C. Andrade, and P. L. de Andres, *Phys. Rev. B* **78**, 014113 (2008).
- ¹⁸ J. Sanchez, J. Fullea, C. Andrade, and P. L. de Andres, *Phys. Rev. B* **81**, 132102 (2010).
- ¹⁹ S. Taketomi, R. Matsumoto, and N. Miyazaki, *Act. Mat.* **56**, 3761 (2008).

- ²⁰ A. Ramasubramaniam, M. Itakura, M. Ortiz, and E. A. Carter, *J. Mater. Res.* **23**, 2757 (2008).
- ²¹ C. S. Becquart, C. Domain, U. Sarkar, A. DeBacker, and M. Hou, *J. Nucl. Mater.* **403**, 75 (2010).
- ²² E. Clouet, S. Garruchet, H. Nguyen, M. Perez, and C. S. Becquart, *Acta Mat.* **56**, 3450 (2008).
- ²³ V. G. Gavriljuk, V. N. Shivanyuk, and B. D. Shanina, *Acta Mat.* **53**, 5017 (2005).
- ²⁴ T.-Y. Zhang, F.-X. Jiang, W.-Y. Chu, and C.-M. Hsiao, *Metall. Trans. A* **16A**, 1655 (1985).
- ²⁵ M. Ortiz and J. Ovejero-Garcia, *J. Mater. Sci.* **27**, 6777 (1992).
- ²⁶ G. Kresse and J. Hafner, *Phys. Rev. B* **48**, 13115 (1993).
- ²⁷ G. Kresse and J. Furthmüller, *Comput. Mat. Sci.* **6**, 15 (1996).
- ²⁸ G. Kresse and J. Furthmüller, *Phys. Rev. B* **54**, 11169 (1996).
- ²⁹ P. Blöchl, *Phys. Rev. B* **50**, 17953 (1994).
- ³⁰ G. Kresse and D. Joubert, *Phys. Rev. B* **59**, 1758 (1999).
- ³¹ J. P. Perdew and Y. Wang, *Phys. Rev. B* **45**, 13244 (1991).
- ³² S. H. Vosko, L. Wilk, and M. Nusair, *Can. J. Phys.* **58**, 1200 (1980).
- ³³ J. P. Perdew, K. Burke, and M. Ernzerhof, *Phys. Rev. Lett.* **77**, 3865 (1996).
- ³⁴ T. C. Leung, C. T. Chan, and B. N. Harmon, *Phys. Rev. B* **44**, 2923 (1991).
- ³⁵ M. Cerny, J. Pokluda, M. Sob, M. Friak, and P. Sanderá, *Phys. Rev. B* **67**, 035116 (2003).
- ³⁶ F. D. Murnaghan, *Proc. Natl. Acad. Sci. USA* **30**, 244 (1944).
- ³⁷ H. C. Herper, E. Hoffmann, and P. Entel, *Phys. Rev. B* **60**, 3839 (1999).
- ³⁸ D. M. Clatterbuck, D. C. Chrzan, and J. W. Morris Jr., *Acta Mat.* **51**, 2271 (2003).
- ³⁹ L. Stixrude, R. E. Cohen, and D. J. Singh, *Phys. Rev. B* **50**, 6442 (1994).
- ⁴⁰ X. Sha and R. E. Cohen, *Phys. Rev. B* **73**, 104303 (2006).
- ⁴¹ J. A. Rayne and B. S. Chandrasekhar, *Phys. Rev.* **122**, 1714 (1961).
- ⁴² M. Acet, H. Zahres, E. F. Wassermann, and W. Pepperhoff, *Phys. Rev. B* **49**, 6012 (1994).
- ⁴³ F. Birch, *Phys. Rev.* **71**, 809 (1947).
- ⁴⁴ D. C. Wallace, *Thermodynamics of Crystals* (Dover, 1972).
- ⁴⁵ T. H. K. Barron and M. L. Klein, *Proc. Phys. Soc.* **85**, 523 (1965).
- ⁴⁶ M. W. Guinan and D. N. Beshers, *J. Phys. Chem. Solids* **29**, 541 (1968).
- ⁴⁷ S. Klotz and M. Braden, *Phys. Rev. Lett.* **85**, 3209 (2000).
- ⁴⁸ A. K. Singh, H. K. Mao, J. Shu, and R. J. Hemley, *Phys. Rev. Lett.* **80**, 2157 (1998).
- ⁴⁹ H. Kimizuka, S. Ogata, J. Li, and Y. Shibutani, *Phys. Rev. B* **75**, 054109 (2007).
- ⁵⁰ J. Wang, J. Li, S. Yip, S. Phillpot, and D. Wolf, *Phys. Rev. B* **52**, 12627 (1995).
- ⁵¹ H. Ma, S. L. Qiu, and P. M. Marcus, *Phys. Rev. B* **66**, 024113 (2002).
- ⁵² P. M. Marcus, H. Ma, and S. L. Qiu, *J. Phys.: Cond. Mat.* **14**, L525 (2002).
- ⁵³ P. M. Marcus and S. L. Qiu, *J. Phys.: Cond. Mat.* **21**, 115401 (2009).
- ⁵⁴ K. Caspersen, A. Lew, M. Ortiz, and E. A. Carter, *Phys. Rev. Lett.* **93**, 115501 (2004).
- ⁵⁵ X. Sha and R. E. Cohen, *Phys. Rev. B* **74**, 214111 (2006).
- ⁵⁶ L. Vocadlo, G. A. de Wijs, G. Kresse, M. Gillan, and G. D. Price, *Faraday Discuss.* **106**, 205 (1997).
- ⁵⁷ J. J. Adams, D. S. Agosta, R. G. Leisure, and H. Ledbetter, *J. App. Phys.* **100**, 113530 (2006).
- ⁵⁸ P. Söderlind, J. A. Moriarty, and J. M. Wills, *Phys. Rev. B* **53**, 14063 (1996).
- ⁵⁹ D. N. Beshers, *J. Appl. Phys.* **36**, 290 (1965).
- ⁶⁰ M. J. Mehl, J. E. Osburn, D. A. Papaconstantopoulos, and B. M. Klein, *Phys. Rev. B* **41**, 10311 (1990).
- ⁶¹ S. Taketomi, R. Matsumoto, and N. Miyazaki, *Int. J. Mech. Sci.* **52**, 334 (2010).
- ⁶² J. O. Bockris, W. Beck, M. A. Genshaw, P. K. Subramanyan, and F. S. Williams, *Acta Metall.* **19**, 1209 (1971).
- ⁶³ O. Buck, L. A. Ahlberg, L. J. Graham, G. A. Alers, C. A. Wert, and K. C. Hsieh, *physica status solidi (a)* **55**, 223 (1979).
- ⁶⁴ G. R. Speich, A. J. Schwoeble, and W. C. Leslie, *Metall. Trans.* **3**, 2031 (1972).
- ⁶⁵ R. Hill, *J. Mech. Phys. Solids* **11**, 357 (1963).
- ⁶⁶ E. Lunarska, A. Zielinski, and M. Smialowski, *Acta Metall.* **25**, 305 (1977).
- ⁶⁷ H. Matsui, H. Kimura, and S. Moriya, *Mater. Sci. Eng.* **40**, 207 (1979).
- ⁶⁸ Y. Murakami, T. Kanezaki, and Y. Mine, *Metall. Mat. Trans. A* **41A**, 2548 (2010).
- ⁶⁹ D. Hull and D. J. Bacon, *Introduction to Dislocations* (Butterworth Heinemann, 2001), 4th ed.
- ⁷⁰ J. P. Hirth and J. Lothe, *Theory of Dislocations* (Krieger Pub. Co., 1992), 2nd ed.
- ⁷¹ J. Turley and G. Sines, *J. Phys. D: Appl. Phys.* **4**, 264 (1971).